




Flame-retardant effect of hyperbranched phosphazene-based microspheres in poly(L-lactic acid)

Xiaoyu Sun¹, Lingling Li¹, Yubin Yang¹, Chunfeng Jia¹, Xiaolei Zhang¹, Jingxuan Wu¹, Zhe Zhu^{1,*}, Junsheng Wang^{2,*}, and Jinjun Yang^{1,3,*} 

¹Tianjin Key Laboratory of Hazardous Waste Safety Disposal and Recycling Technology, School of Environmental Science and Safety Engineering, Tianjin University of Technology, 391 Binshui Xidao, Xiqing District, Tianjin 300384, China

²Tianjin Fire Research Institute of the Ministry of Emergency Management, Tianjin 300381, China

³Suzhou Qichu Intelligent Technology Co., Ltd., 25-6-418B-64 Lushan Road, Gaoxin District, Suzhou, China

Received: 21 August 2021

Accepted: 11 November 2021

Published online:
3 January 2022

© The Author(s), under exclusive licence to Springer Science+Business Media, LLC, part of Springer Nature 2021

ABSTRACT

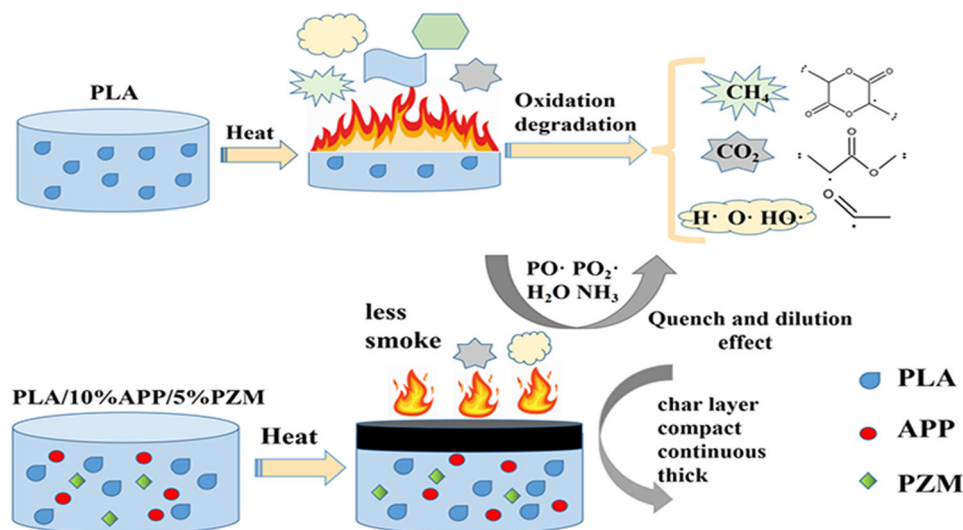
A hyperbranched and amorphous microsphere (PZM) was synthesized with the hexachlorocyclotriphosphazene (HCCP) as the component unit. The PZM and ammonium polyphosphate (APP) as a synergistic flame retardant were incorporated into the poly(L-lactic acid) (PLA) to investigate the effects of the APP/PZM on the thermal stability, limiting oxygen index (LOI), UL-94 rating, combustion behavior, flame-retardant performance and crystallization behavior of the PLA. The PZM showed a much higher thermal stability and carbon residue than the HCCP, APP and 4,4'-diaminodiphenyl ether (ODA), but presented a lower initial degradation temperature. The PLA/10%APP/5%PZM exhibited the most excellent flame-retardant performance because it showed low total heat release, peak of heat release and total smoke release. By calculation, the PLA/10%APP/5%PZM presented the outstanding fire resistance. The PLA/10%APP/5%PZM formed a continuous, dense and relatively thicker char layer (which facilitated the isolation of the oxygen and heat flow, suppression of the smoke and prevention of the dripping) after the cone calorimeter (CONE) test, indicating that it showed a condensed-phase flame-retardant performance. In addition, the gas-phase flame retardance is a minor factor to enhance its flame-retardant effect. The crystallizability increased, and crystallization time shortened substantially for the PLA with loading of the 10%APP/5%PZM.

Handling Editor: Maude Jimenez.

Xiaoyu Sun and Lingling Li contributed equally to this work as co-first authors.

Address correspondence to E-mail: zhuzhe@tjut.edu.cn; wangjunsheng@tfri.com.cn; tjyjj_2014@tjut.edu.cn

GRAPHICAL ABSTRACT



Introduction

More and more attention has been paid on the poly(L-lactic acid) (PLA) due to the severe environmental pollution caused by the traditional petroleum-based non-biodegradable plastic. The PLA is a kind of biodegradable, compatible, bio-derived, renewable and sustainable polyester material and shows good mechanical properties, transparency and processing performance [1–8]. The PLA can be synthesized by the polymerization of lactic acid produced via the fermentation of the corn, sugar beet, cassava and other plants [9, 10]. The PLA-based composites have been extensively applied in the biomedical devices, automotive parts, food packings, disposable containers and bags. However, the raging flame and severe dripping appear during the combustion process of the PLA-based composites, accompanied with the substantial toxic gases. Therefore, from the viewpoint of the fire safety, the flammability of the PLA is always a challenging issue to be resolved [11–14].

Several methods have been used for increasing the flame retardance of the PLA. The surface of the PLA was treated/coated by the flame retardant (FR), but the preparation is relatively complicated [15–19].

Wang et al. developed a new method for preparing the flame-retardant PLA via the chemical grafting of the FR monomer to the PLA molecular chain [20]. They used the reactive FR (ethyl phosphorous dichloride) as a chain extender of the main chain to synthesize phosphorus-containing PLA (PPLA). Upon incorporation of 5 wt% PPLA into the PLA matrix, the V-0 rating (UL-94 combustion test) and limit oxygen index (LOI) of 25% are achieved for the PLA-based composite, an indicative of good flame retardance of the PPLA. However, the complicated synthesis routes, well-controlled reaction conditions and higher time cost are involved. Addition of the FR into the polymer matrix via the melt blending is an efficient, facile, cost-effective, time-saving and extensively used approach to prepare the polymeric composite with flame retardance. Wang et al. studied the influence of phosphorus-based FRs on the combustion performance of the PLA by direct melting mixing the aryl polyphenylphosphonic acid (WLA-3) and PLA [21]. The experimental results suggest that the self-extinguishing occurs for the PLA/7wt% WLA-3. The UL-94 combustion test reaches the V-0 rating, and the corresponding LOI is 25%.

Recently, it has been reported that some compounds containing the phosphazene group have good flame retardancy and reduce the toxicity of the

PLA in the combustion process. Hexachlorocyclotriphosphazene (HCCP) is a derivative containing the phosphazene with the $-P=N-$ unit as a skeleton and exhibits the super flame retardancy and self-extinguishing properties [22, 23]. The HCCP has been used to synthesize the nano- and microscale polymers through the polycondensation reaction, such as polyphosphazene nanotubes, microspheres, nano-chains and nanofibers [24, 25]. These nanomaterials have high thermal stability, flame retardancy and radiation resistance [26, 27]. Li, Wang and co-workers synthesized a new type of FR (HPCA) with a hyperbranched structure using synthetic cyanuric chloride and 4,4'-diaminodiphenyl sulfide [26]. The HPCA and ammonium polyphosphate (APP) as a synergistic FR (HPCA/APP) increase the flame retardance of the PLA.

Chen et al. synthesized a flame-retardant HTTCP containing phosphazene and triazine groups. When the mass fraction of HTTCP was 25 wt %, the PLA composite acquired a LOI value of 25.2% and the lower pHRR of 290 kW/m² [28]. They also used nano-zinc oxide (nano-ZnO) and phosphazene/triazine bi-group flame-retardant doped in situ with nano-zinc oxide (A4-d-ZnO), and the results show that PLA/5%A4-d-ZnO composite presents a LOI value of 24% and pHRR of 501 kW/m² and reaches the V-2 rating. A LOI value of 36% achieves for the PLA composite containing intumescent FR (IFR)/A4-d-ZnO [29, 30]. In addition, a micro-cross-linked structure was constructed via addition of zinc oxide with the nano-ZnO and chain extender (ADR) into the FRPLA. When 0.8% ADR/1% ZnO is added, the LOI value of the FRPLA reaches 39.4%. Compared with neat PLA, the pHRR and THR reduce by 60% and 43%, respectively, showing an excellent flame-retardant effect [31].

Motivated by the reports aforementioned, we prepared a novel HCCP-based derivative as a high-efficiency FR (PZM) of the PLA with a simple and efficient method. The PZM was synthesized using the 4,4'-diaminodiphenyl ether (ODA) bearing the benzene ring and HCCP, presenting the hyperbranched network-like structure (as displayed in Scheme 1). Moreover, in our present work, the PZM showed the microsphere structure (Fig. 1) which was seldomly reported on the HCCP-based derivative. The FR with the microsphere structure is anticipated to be beneficial to enhance the flame retardance. Additionally, the FR bearing the benzene can enhance substantially

the char-forming ability of the PLA [32–37]. The chlorine (Cl) of the HCCP reacts readily with the $-NH_2$ group of the ODA to obtain the halogen-free PZM to reduce the emission of the toxic gas during the pyrolysis or combustion process, as much as possible. The hyperbranched structure of the PZM (as shown in Scheme 1) in which the HCCP and ODA are cross-linked, probably exhibits an outstanding flame retardance [38]. To further enhance the flame retardance of the PLA, the PZM and intumescent APP FR were used as a synergistic FR to investigate its flame-retardant effect on the PLA. It should be mentioned that the extremely low crystallizability or long processing cycle is also a bottleneck for the processing of the PLA. Hence, the PZM/APP synergistic FR is also anticipated to accelerate the crystallization rate and shorten the crystallization time of the PLA. In this work, the chemical structure of synthesized PZM was characterized by Fourier-transform infrared (FTIR), wide-angle X-ray diffraction (WAXD) and X-ray photoelectron spectroscopy (XPS). The LOI, thermogravimetric analysis (TGA), UL-94 vertical burning and cone calorimeter test were utilized to investigate the flame retardance and thermal properties of the composite. The DSC measurement was performed to investigate the crystallizability of the PLA-based composite. The morphology observation was carried out on the scanning electron microscopy (SEM).

Experimental

Materials

The PLA (4032D, Natureworks, $M_w = 96,000$ Da) was supplied from Cargill Dow Inc. (USA). Both the HCCP and ODA were purchased from Shanghai Maclean Biochemical Technology Co., Ltd. (China). The APP was purchased from Taixing Fine Chemical Co., Ltd. (China). The pyridine was bought from Shanghai Chunjing Biochemical Technology Co., Ltd. (China). The sample/reagents are used as received without the further purification.

Preparation of the PZM

According to the previous literature [39], the synthesis routes of the PZM are described as follows. The ODA (15.59 g, 0.078 mol) was added in 300 ml pyridine in the ice bath, well stirred and treated by the

Table 1 Composition of samples

Sample	Composition (wt%)		
	PLA (wt%)	APP (wt%)	PZM (wt%)
PLA	100	0	0
PLA/5wt%APP	95	5	0
PLA/10wt%APP	90	10	0
PLA/5wt%PZM	95	0	5
PLA/10wt%PZM	90	0	10
PLA/5wt%APP/5wt%PZM	90	5	5
PLA/10wt%APP/5wt%PZM	85	10	5
PLA/5wt%APP/10wt%PZM	85	5	10
PLA/10wt%APP/10wt%PZM	80	10	10

The mass loss of the sample was carried out using the thermogravimetric analysis (TGA, Shanghai Yunou Industrial Co., Ltd., China). The sample was heated from 25 to 600 °C at a rate of 10 °C/min in the presence of nitrogen atmosphere (with a N₂ flow of 100 mL/min). Before the measurement, the sample was completely dried in the vacuum.

The vertical combustion (UL-94) test was performed on a TTech-GBT2408 Tester (Suzhou Testech Testing Instrument Technology Co., Ltd., China) according to the ATSM D3801-2010 standard. The average value of 5 independent samples (with the size of 130 × 13 × 3 mm³) was recorded for the analysis.

The limiting oxygen index (LOI) experiment was measured on an oxygen index meter (JF-3, Nanjing Jiangning Analytical Instrument Co., Ltd., China) according to the ASTM D2863-2013 standard. The average value of 5 independent samples (with the size of 130 × 6.5 × 3 mm³) was recorded for the analysis.

Dual cone calorimeter (EN ISO 1716, FTT, Technology Limited, UK) with a heat flux of 35 kW/m² was used for a measurement of the combustion behavior of the sample. The average value of 3 independent samples (with the size of 100 × 100 × 3 mm³ according to the ISO 5660-1 standard) was recorded for the analysis.

Thermogravimetric analysis/Fourier-transform infrared (TG-FTIR) measurement was performed on a STA6000-Frontier instrument (PerkinElmer, USA). The sample was heated from 25 to 700 °C at a rate of 10 °C/min under the N₂ atmosphere, with a resolution of 2 cm⁻¹ and an accumulation of 32 scans.

Scanning electron microscope–energy-dispersive spectrometer (SEM–EDS) test was performed on a

scanning electron microscope (SU 3500, Hitachi, Japan), with an acceleration voltage of 15 kV and a working distance of 40–50 mm.

Pyrolysis–gas chromatography/mass spectrometry (PY-GC/MS) analysis was conducted on a CDS5200/Clarus680SQ8T apparatus (CDS-PerkinElmer, USA). The sample temperature, GC/MS interface temperature and cracker temperature were set to 40, 280 and 500 °C, respectively, and the heating rate is 10 °C/min. The helium was used as the carrier gas. The capillary column with 30 m length, inner diameter of 0.25 mm and a liquid film thickness of 0.25 μm were utilized for the test.

The non-isothermal/isothermal cooling and heating curves were recorded on a Pyris Diamond differential scanning calorimeter (DSC, Netzsch, Germany). The sample was heated from –30 to 190 °C at a rate of 10 °C/min to erase the thermal history. Regarding the non-isothermal crystallization, the molten sample was slowly cooled to –30 °C at a rate of 10 °C/min. With respect to the isothermal crystallization, the molten sample was quenched to a given melt crystallization temperature (*T_c*) for a long enough time period. After the non-isothermal/isothermal crystallization, the sample was reheated to 190 °C.

The tensile test of neat PLA and PLA-based composites was carried out using a SUNS UTM2503 (Shenzhen, China) tensile equipment with a rate of 10 mm/min at the room temperature. For each given material, 5 independent specimens were measured. The dumbbell sample (with 50 mm length, 25 mm cross section width and 0.8 mm thickness) was cut, and the average value was recorded to evaluate the mechanical property (tensile strength and elongation at break).

Results and discussion

Characterization of the PZM

Figure 1 shows the SEM image and atomic percentages of the PZM. It reveals that the PZM has the well-defined microspheres with the diameter of 2.3–6.8 μm . The table embedded in Fig. 1 shows the atomic percentages in the PZM which were obtained from the XPS measurement. The atomic ratio of the P and O is 6.84%:13.37% (which is close to 1:2). As presented in Scheme 1, if 6 Cl atoms of 1 mol HCCP are completely replaced by the $-\text{NH}_2$ group of 6 mol ODA, the synthetic PZM (with the hyperbranched structure) shows a P/O atomic ratio of 1:2. The experimental result is in good agreement with our expectation. Figure 2 shows the IR spectra of the HCCP, ODA and PZM. The two peaks at 527 and 607 cm^{-1} (assigned to the P-Cl group of the HCCP [37]) disappeared in the PZM. The peak at 862 cm^{-1} attributed to the P-N segment of the HCCP [37] disappeared, and two new ones at 926 and 821 cm^{-1} appeared in the PZM, probably associated with the newly formed P-N group of the PZM. The discrepancy of the peak position of the P-N segment of the cyclotriphosphazene between the HCCP and PZM should be related to the difference of the molecular microenvironment. The above IR results suggest that the PZM was synthesized successfully. In addition, two characteristic peaks at 1504 and 1627 cm^{-1} are ascribed to the bending vibration of N-H bond in the ODA and PZM. Those peaks higher

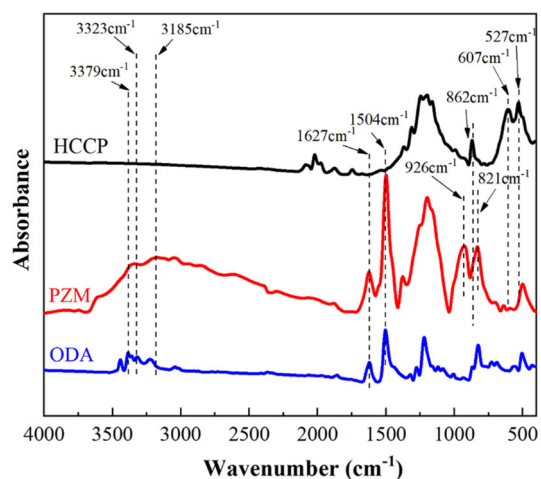


Figure 2 The FTIR spectra of the HCCP, ODA and PZM.

than 3100 cm^{-1} in the ODA and PZM are assigned to the $-\text{NH}_2$ or $-\text{NH}-$ groups [37, 39].

Figure 3 shows the WAXD patterns of the HCCP, ODA and PZM. Both the HCCP and ODA exhibit many sharp diffraction peaks, indicating they possess the polycrystalline crystal structure. However, no diffraction peak is discernible in the PZM, revealing that the PZM is amorphous. Similar results were reported on the HCCP-based derivative. It confirms again that the PZM was synthesized successfully.

Figure 4 displays the XPS spectra of the HCCP, ODA and PZM. The HCCP showed three main peaks assigned to the P2p and Cl2p and N1s, respectively, and the ODA presented three ones related to the C1s, N1s and O1s, respectively. Four predominant peaks attributed to the P2p, C1s, N1s and O1s, respectively, appeared in the PZM, and their positions changed little. It is noteworthy that there was no peak associated with the Cl2p in the PZM, indicating that the PZM is a halogen-free compound.

Peak fitting performed on the XPS spectra of the HCCP, ODA and PZM is shown in Fig. 5. Two peaks locating at 399.5 and 401.3 eV are associated with the P=N and P-N of the HCCP, respectively (Fig. 5a1), and two ones at 398.9 and 399.6 eV are related to the C-N and $-\text{NH}_2$ of the ODA, respectively (Fig. 5a2). A new peak at 399.8 eV is assigned to the $-\text{NH}-$ of the PZM (5a3) [40, 41]. In Fig. 5b1 and b2, those four peaks at 284.6, 285.6, 286.2 and 290.6 eV are related to the C-H, C-N, C-O and $\pi-\pi$, respectively, of the ODA and PZM [42]. In Fig. 5c1, those three peaks at 133.2, 133.4 and 133.5 eV correspond to the P=N, P-Cl and P-N, respectively, of the HCCP [39]. In

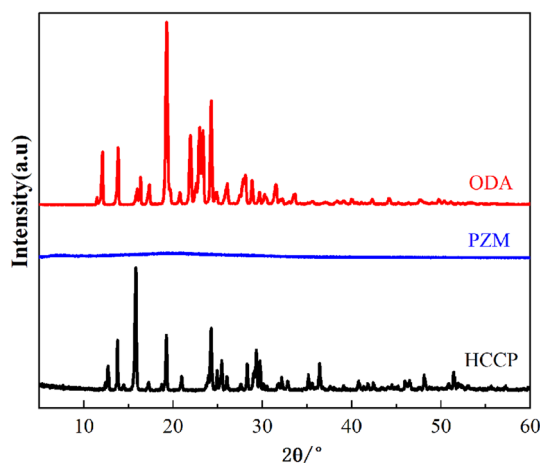


Figure 3 The WAXD patterns of the HCCP, ODA and PZM.

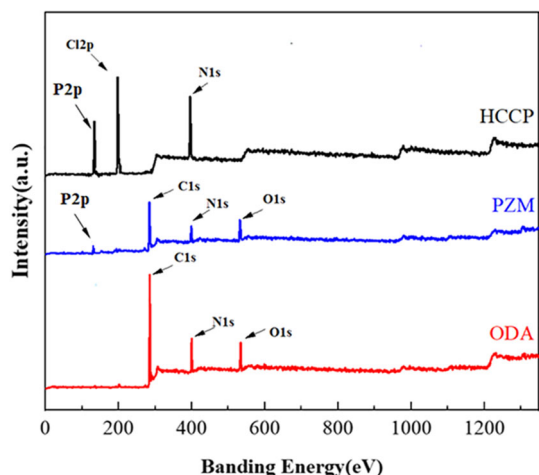


Figure 4 The XPS spectra of the HCCP, ODA and PZM.

Fig. 5c2, that of the P–Cl segment disappeared in the PZM.

Thermal stability analysis

The TGA and DTG curves of the HCCP, ODA, APP and PZM under the nitrogen atmosphere are

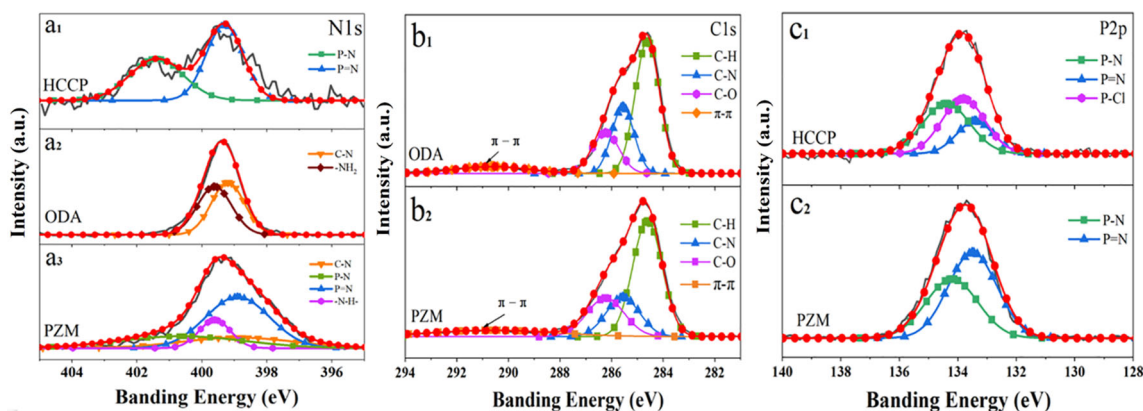
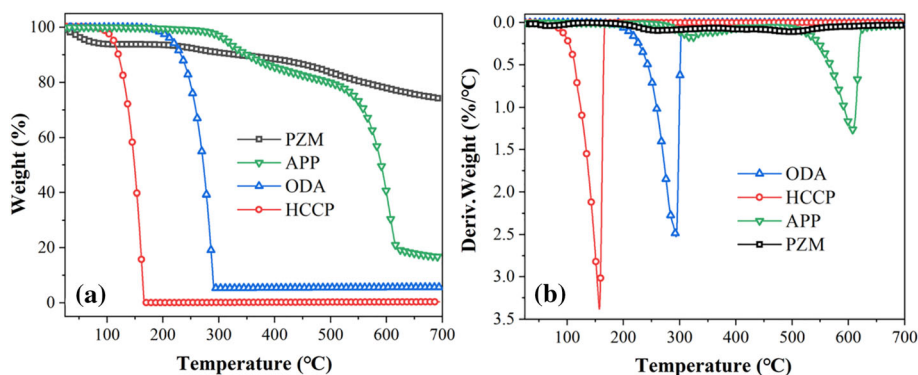


Figure 5 High-resolution XPS spectra of the HCCP, ODA and PZM.

Figure 6 **a** TGA and **b** DTG curves of the HCCP, ODA, APP and PZM under the N_2 atmosphere.



presented in Fig. 6. Several typical data are listed in Table S1. Both the HCCP and ODA degraded in one-step mode (Fig. 6a, b). Their initial thermal degradation temperatures ($T_{5\%}$) are 112 and 216 °C, respectively. The temperature at which the degradation rate is the maximum (T_{max}) of the HCCP and ODA is 168.1 and 291.5 °C (Fig. 6b), respectively, and presented the residue percentage of 0.4% and 5.7% (Table S1), respectively. The APP was thermally degraded in two-step manner (Fig. 6b). The first degradation stage between 315 and 514 °C mainly resulted from the decomposition of the APP to generate the NH_3 , H_2O and polyphosphoric acid. The second stage higher than 520 °C was attributed to the degradation of the polyphosphoric acid to produce the phosphoric acid and phosphorus-containing fragments. In Table S1, the PZM displayed a lowest $T_{5\%}$ (95 °C, ascribed to the evaporation of the water probably due to the good hygroscopicity) and highest residue percentage (74.2%, probably attributed to the excellent char-forming ability of the hyperbranched structure), compared to the HCCP, ODA and APP.

LOI and UL-94 measurement

The test data in the LOI and UL-94 measurement are listed in Table 2. Neat PLA showed the LOI value of 20% and no rating in the UL-94 test because the severe dripping ignited the degreasing cotton. With loading of the APP, PZM or APP/PZM, the PLA-based composites presented the increased LOI values. Additionally, except the PLA/5wt%APP, other PLA-based composites passed the UL-94V-0 test, indicating that these FRs showed a good flame-suppressing effect on the PLA. By contrast, the PLA/10%APP/5%PZM showed a distinct self-extinguishing effect after being ignited, but neat PLA was burnt thoroughly, as presented in the video of Supplementary Material (V_{PLA} and $V_{PLA-10\%APP-5\%PZM}$).

Thermal stability of neat PLA and PLA-based composites

The TGA and DTG curves of neat PLA and PLA-based composites under the N_2 atmosphere are shown in Fig. 7, and the corresponding data are listed in Table S2. Compared to neat PLA, the $T_{5\%}$ decreased slightly and progressively with an increase in the amount of the FR because of the breakage of the PLA molecular chains which are in contact with the phosphoric acid-containing compound gas. The T_{max} changed little for the PLA-based composites. The char residue percentage of the PLA/APP/PZM is obviously higher than those of the neat PLA and PLA/APP, indicating that the synergistic effect of the APP/PZM enhanced the char-forming capacity of the PLA. The maximum mass loss rate (MMLR) of neat PLA is higher than other PLA/FRs (with exception of the PLA/10%APP), probably related to the lower $T_{5\%}$ and higher char residue percentage of the PLA/FRs.

Combustion behavior investigated by the CONE

The CONE test is widely utilized to simulate the real fire environment and evaluate combustion behavior of materials. Figure 8a displays the heat release rate (HRR) curves with the combustion time for neat PLA and PLA-based composites. Upon incorporation of the FRs, the heat release rate (HRR) decreased obviously and the time at which the maximum HRR (pHRR) appears, also reduced, probably associated with the depression of the thermal degradation temperature of the FRs, in agreement with the results in Fig. 7. Among those 9 samples, the PLA/10%APP/5%PZM (PLA-7) showed the lowest pHRR and decreased by 27.2% compared to neat PLA, as presented in Fig. 8b and Table 3. Also, it suggests that the 10%APP/5%PZM synergistic FR exhibited the relatively better inhibition effect on the heat release, compared to the 10%APP or 5%PZM.

Similarly, the total heat release (THR) slowed down upon incorporation of the FRS and the PLA/10%APP/5%PZM displayed the lowest THR, as presented in Fig. 9a. The PLA/10%APP/5%PZM and PLA/10%APP showed substantially lower total smoke release (TSR) than neat PLA and other composites (Fig. 9b and Table 3). The PLA/10%APP/5%PZM and PLA/10%APP presented excellent smoke-suppressing effect (Fig. 9b). Due to the earlier decomposition of the APP (or lower thermal stability than the PZM, as shown in Fig. 6), the released phosphorus-containing free radicals ($PO\cdot/PO_2\cdot$) can capture and quench free radicals (such as $O\cdot, HO\cdot$) generated in the combustion process of the PLA, suppressing the generation of the thermally degraded gas product. The lowest TSR of the PLA/

Table 2 The LOI and UL-94 test data

Code	Sample	LOI (%)	UL-94		
			Dripping	Ignition	Rating
PLA-1	PLA	20.0	Yes	Yes	No rating
PLA-2	PLA/5wt%APP	25.4	Yes	No	V-2
PLA-3	PLA/10wt%APP	27.2	No	No	V-0
PLA-4	PLA/5wt%PZM	24.0	No	No	V-0
PLA-5	PLA/10wt%PZM	26.0	No	No	V-0
PLA-6	PLA/5wt%APP/5wt%PZM	27.4	No	No	V-0
PLA-7	PLA/10wt%APP/5wt%PZM	27.6	No	No	V-0
PLA-8	PLA/5wt%APP/10wt%PZM	28.0	No	No	V-0
PLA-9	PLA/10wt%APP/10wt%PZM	28.2	No	No	V-0

Figure 7 a TGA and b DTG curves as a function of temperature for neat PLA and PLA-based composites under N₂ atmosphere.

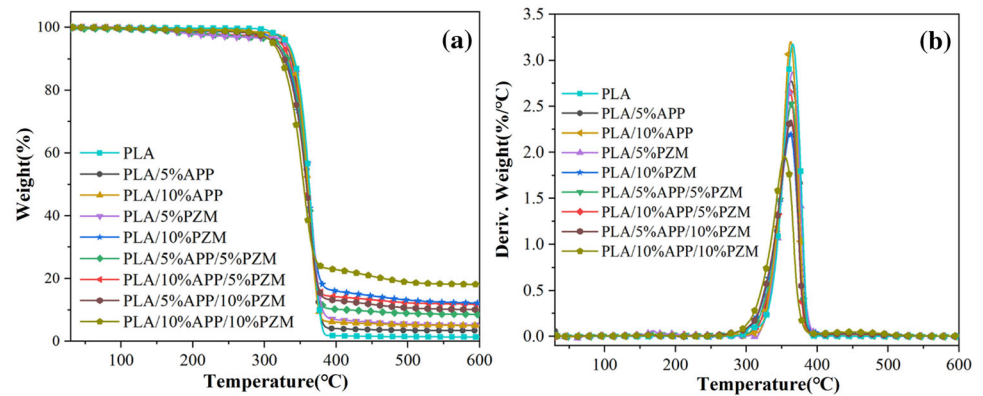


Figure 8 The HRR versus combustion time for neat PLA and PLA-based composites.

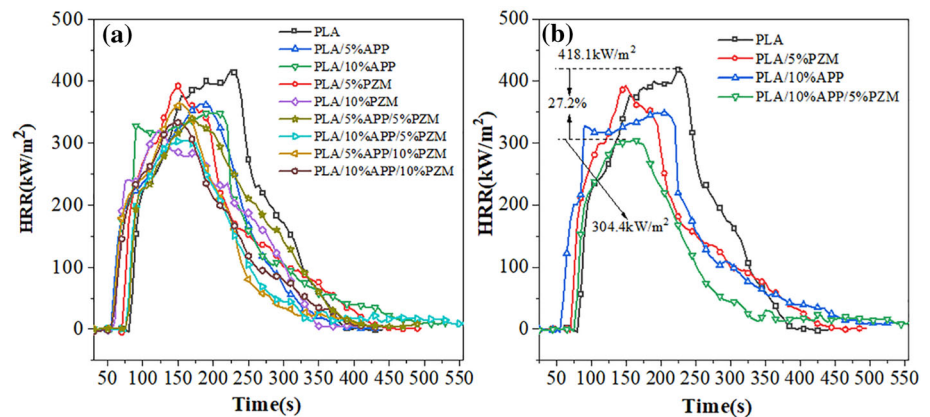


Table 3 Combustion parameters of neat PLA and its composites from the cone calorimeter

Sample	TTI (s)	pHRR (kW/m ²)	THR (MJ/m ²)	TSR (m ² /m ²)	av-EHC (MJ/kg)	FPI (sm ² /kW)	FRI
PLA	79 ± 4	418 ± 11	72 ± 8	22.2 ± 1.2	18.4 ± 0.6	0.19 ± 0.02	1
PLA/5wt%APP	50 ± 2	362 ± 13	61 ± 6	4.4 ± 0.3	16.6 ± 0.9	0.13 ± 0.02	0.81 ± 0.11
PLA/10wt%APP	53 ± 3	349 ± 11	57 ± 7	6.1 ± 0.7	15.9 ± 0.9	0.15 ± 0.03	1.01 ± 0.13
PLA/5wt%PZM	67 ± 2	321 ± 13	63 ± 5	14.6 ± 1.1	17.4 ± 0.8	0.17 ± 0.01	1.02 ± 0.12
PLA/10wt%PZM	54 ± 3	392 ± 9	57 ± 8	6.7 ± 0.7	16.1 ± 0.8	0.16 ± 0.02	1.05 ± 0.11
PLA/5wt%APP/5wt%PZM	74 ± 2	339 ± 10	62 ± 6	5.5 ± 0.3	16.8 ± 0.9	0.21 ± 0.03	1.28 ± 0.13
PLA/10wt%APP/5wt%PZM	75 ± 3	304 ± 12	48 ± 4	3.6 ± 0.2	15.3 ± 1.0	0.24 ± 0.03	1.9 ± 0.15
PLA/5wt%APP/10wt%PZM	52 ± 4	363 ± 8	52 ± 7	5.8 ± 0.5	15.8 ± 0.7	0.14 ± 0.04	1.03 ± 0.12
PLA/10wt%APP/10wt%PZM	58 ± 5	333 ± 13	54 ± 6	5.6 ± 0.3	15.8 ± 0.8	0.17 ± 0.02	1.2 ± 0.14

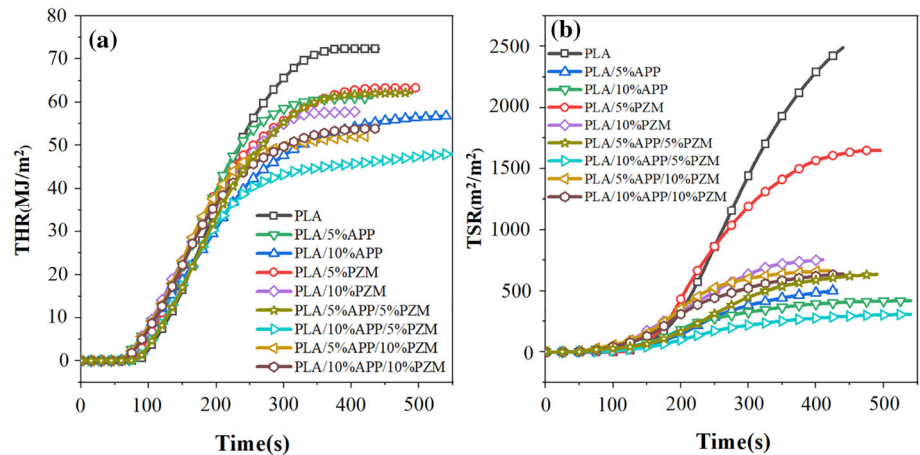
$$\text{FPI} = \text{TTI}/\text{pHRR}$$

$$\text{FRI} = \frac{[\text{THR} \times (\frac{\text{pHRR}}{\text{TTI}})]_{\text{neat PLA}}}{[\text{THR} \times (\frac{\text{pHRR}}{\text{TTI}})]_{\text{PLA composites}}}$$

10%APP/5%PZM is probably attributed to its relatively higher char-forming capability (the residue percentage of 11.9%, as presented in Table S2), inhibiting the emission of the smoke gas.

Additionally, the quenching effect of the phosphorus-containing free radicals in the APP on the O·/HO·-free radicals is also an important factor to lower the emission of smoke gas.

Figure 9 a THR and b TSR versus combustion time for neat PLA and PLA-based composites.



The time to ignition (TTI) is the time from being heated to appearance of stable flame in the CONE test, and it is an important parameter for evaluating the fire resistance of the material. Clearly, the TTI of the PLA/APP depressed greatly compared to neat PLA (Table 3), probably related to the acid products of the APP (suffered from the heat radiation) which accelerate the thermal degradation of the PLA molecular chains caused by the hydroxyl radicals, to enhance the flammability of the PLA. A slight decrease in the TTI was found for the PLA/10%APP/5%PZM (75 S), compared to neat PLA (79 S).

The released heat of the unit mass loss can be expressed by the av-EHC (average effective heat of combustion) in the CONE measurement. From Table 3, with loading of the APP or PZM or APP/PZM, the av-EHC depressed compared to neat PLA and the PLA/10wt%APP/5wt%PZM displayed the lowest av-EHC, revealing the burning degree of volatile gas in the gas-phase flame reduced in the presence of the synergistic FR (APP/PZM). The fire performance index (FPI) is the ratio of the TTI to pHRR, and the larger FPI is an indicative of a longer escape time in the fire [43]. Similarly, the FPI of the PLA-based composites reduced upon incorporation of the FRs and the PLA/10wt%APP/5wt%PZM presented the highest FPI (0.24 sm^2/kW), indicating that the APP/PZM exhibited the synergistic flame-retardant effect on the PLA and the PLA/10wt%APP/5wt%PZM showed the highest fire safety. The FRI parameter is adopted to evaluate the flame-retardant performance of thermoplastic composites, and the larger FRI demonstrates a higher thermal stability of the polymeric material [44]. In Table 3, with loading of the APP, the FRI decreased

or changed little. Blending of the PZM, no apparent alteration could be found. Upon incorporation of the 10%APP/5%PZM, the FRI increased nearly by 1 time, compared to neat PLA.

It is mentioned that the flame-retardant effect of the PLA/10wt%APP/10wt%PZM is not better than the PLA/10wt%APP/5wt%PZM, indicating that more amount of the synergistic FR lowers the flame-retardant performance of the composite, probably related to the weak/poor interfacial interaction between the 10%APP/10%PZM and PLA, or the agglomeration of the synergistic FR with more amount in the PLA matrix, as presented in Fig. S1 (the fracture SEM image of the PLA/10%APP/10%APP composite).

Morphology observation of the char residue

Figure 10 shows the images of the char residue of neat PLA and its composites treated by the CONE test. Neat PLA showed an extremely thin char layer with a large hole, revealing a substantially low flame retardance of neat PLA. In addition, a small hole and relatively thicker char layer were seen in the PLA/5%PZM. Other PLA-based composites showed a continuous, dense and compact layer, indicating that they had the increased flame retardance.

The SEM images of neat PLA and its composites treated by the CONE test are shown in Fig. 11. There are many large cracks on the surface of neat PLA, accelerating the escape of generated CO, CO₂, H₂O and volatile gas product related to breakage of the PLA molecular chains. Small cavities were found in the PLA/5%APP, PLA/10%APP and PLA/5%PZM. The continuous and compact char layer without the pores or cracks could be clearly seen in other

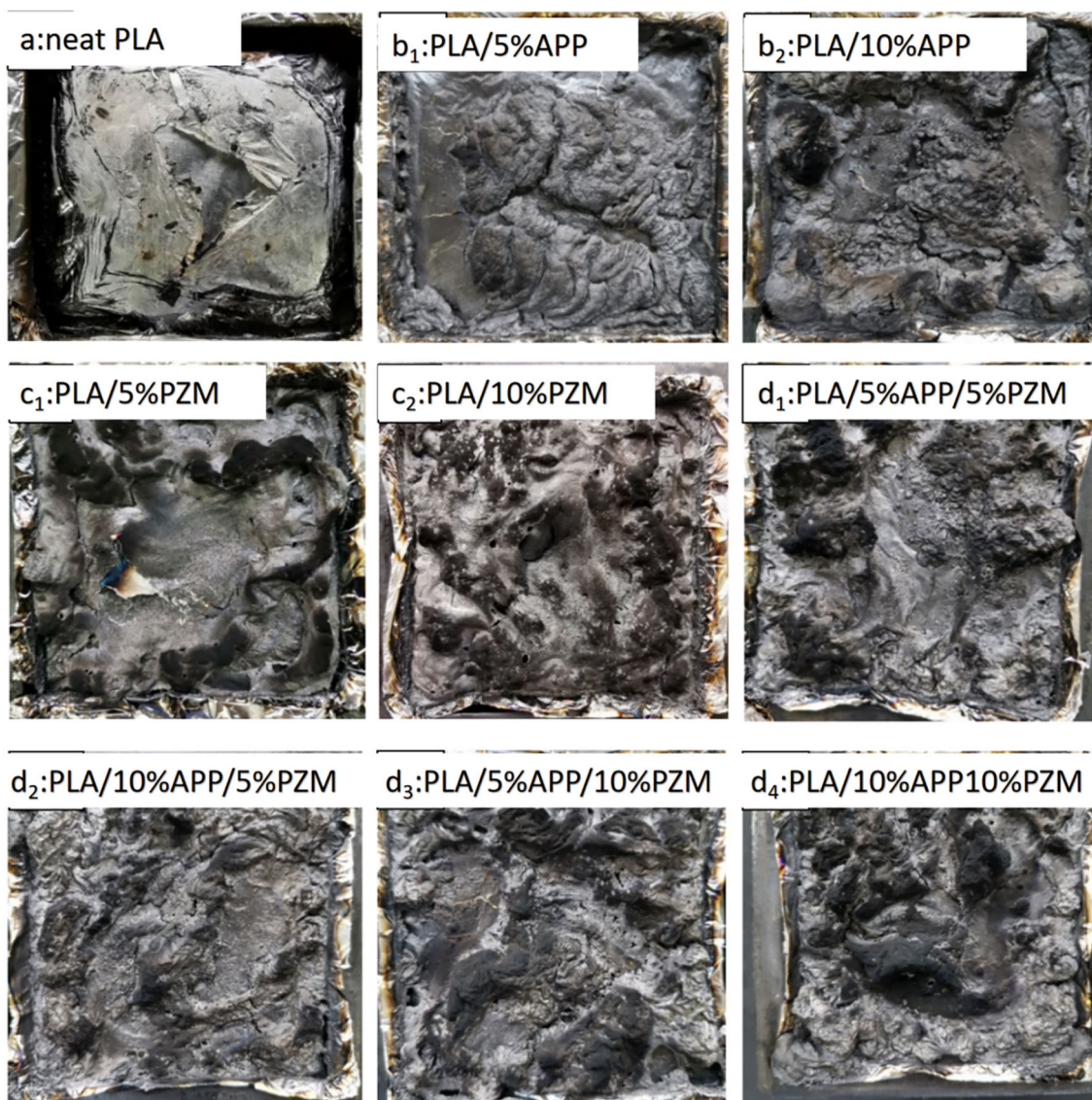


Figure 10 Digital images of the char residue of neat PLA and its composites.

composites, facilitating the isolation of the oxygen and heat, suppression of the smoke and prevention of the dripping.

TG-FTIR measurement

Figure S2 presents the time-dependent TG-FTIR 3D spectra of neat PLA and several PLA-based composites. By contrast, the intensity of main IR absorption peaks (attributed to carbonyl/ester/amide segments) of the PLA/10%APP/5%PZM was lower than those of neat PLA and other two composites, probably ascribed with its highest char residue percentage (compared with neat PLA, PLA/10%APP and PLA/5%PZM), as shown in Table S2. The thicker

carbon layer showed the barrier effect to suppress the evaporation of the smoke or gas product.

Figure 12 displays the FTIR spectra at various temperatures in the TG-IR measurement, and the assignment of the different IR peaks is denoted. On the whole, the IR absorption peak of the composites appeared and disappeared earlier than neat PLA, indicating that thermal degradation of the composites occurred in the lower temperature region, in particular for the PLA/10wt%APP/5wt%PZM, perhaps ascribed to the degradation of the flame retardant in the lower temperature or the intramolecular/intermolecular dehydration of PLA (catalyzed by the acidic substances produced by the degradation of

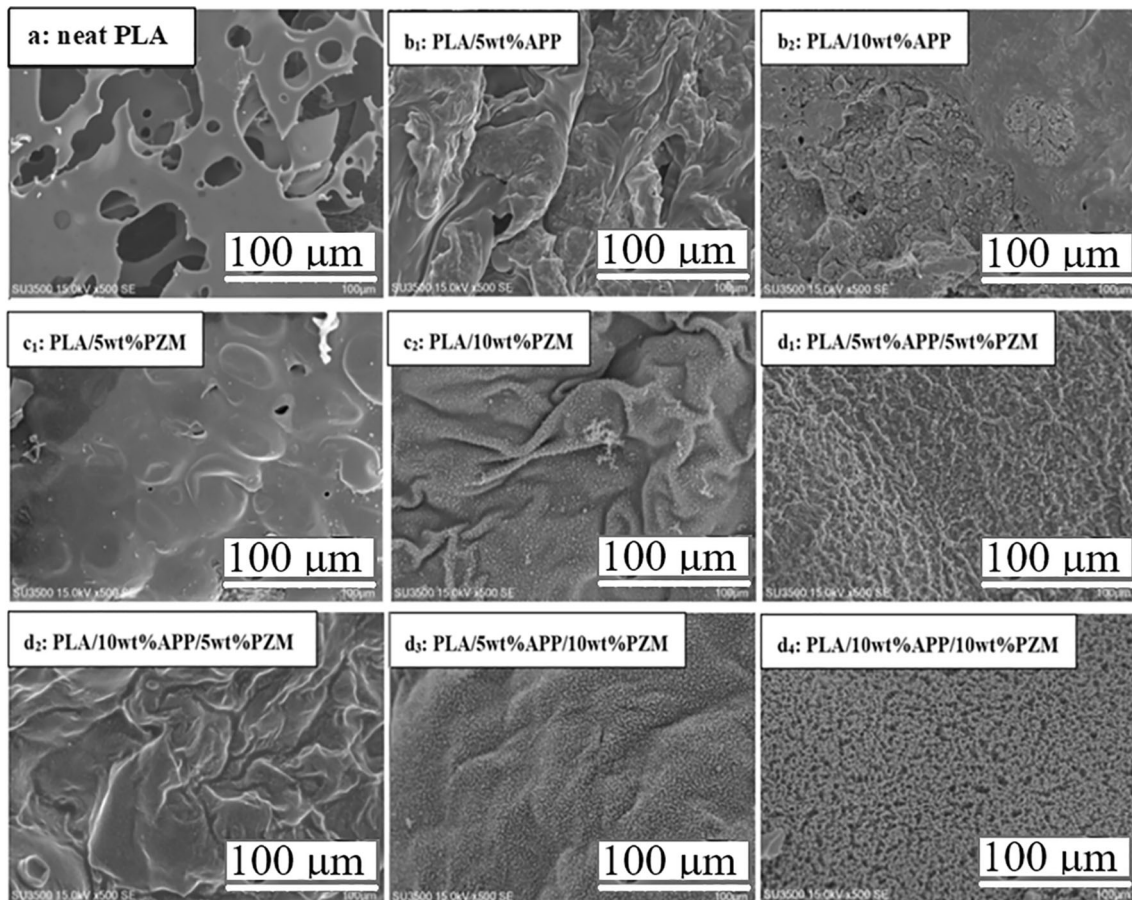


Figure 11 SEM images (zoom in 500 times) of neat PLA and its composites treated by the cone calorimetry test.

APP). This result is consistent with that in the TGA test. The thermal degradation of the 10%APP/5%PZM synergistic retardant at the lower temperature is helpful for the formation of the char layer, which acts as a protective film to enhance the flame retardance of the PLA matrix, because it played an important role in the incomplete combustion, insulation of heat and oxygen [45].

Figure S3 presents the FTIR spectra of the pyrolysis gas-phase products of neat PLA and several composites at T_{max} . Two IR peaks at 3742 and 2731 cm^{-1} are assigned to -OH (H_2O) and alkane gas-phase products. The characteristic peaks of CO_2 appeared at 2361 and 2313 cm^{-1} [46], and both at 2176 and 2105 cm^{-1} are related to CO [47]. That at 1773 cm^{-1} is ascribed to the -C=O group, and these two ones at 1365 and 910 cm^{-1} to the bending vibration of the C-H [48]. Apparently, the intensity of the IR peak of the PLA/10%APP/5%PZM was lower than those of other 3 samples, revealing that the gas-phase pyrolysis products of the PLA/10%APP/5%PZM reduced.

PY-GC/MS analysis

Figure 13 shows the total ion chromatograms of the PZM, neat PLA and PLA /10%APP/5%PZM in the PY-GC/MS measurement, and their corresponding MS chromatograms at different retention times are presented in Fig. 14. With combination of Figs. 13 and 14, the possible pyrolysis products of the PZM, neat PLA and PLA /10%APP/5%PZM (with the time) are shown in Fig. 15a, b and c, respectively. It can be seen from Fig. 15a that the main pyrolysis products of the PZM are the phosphazene group and other phosphorus-/benzene-based derivatives. From Fig. 15b, the main pyrolysis products of neat PLA are the lactide, CO_2 , cyclic and carbonyl compounds. As presented in Fig. 15c, the phosphazene group and benzene-based derivatives, lactide and carbonyl compounds are the main pyrolysis volatile products. In the decomposition process, the benzene- and phosphorus-containing free radicals can quickly capture and quench the $\text{O}\cdot$, $\text{H}\cdot$, $\text{HO}\cdot$ free radicals of

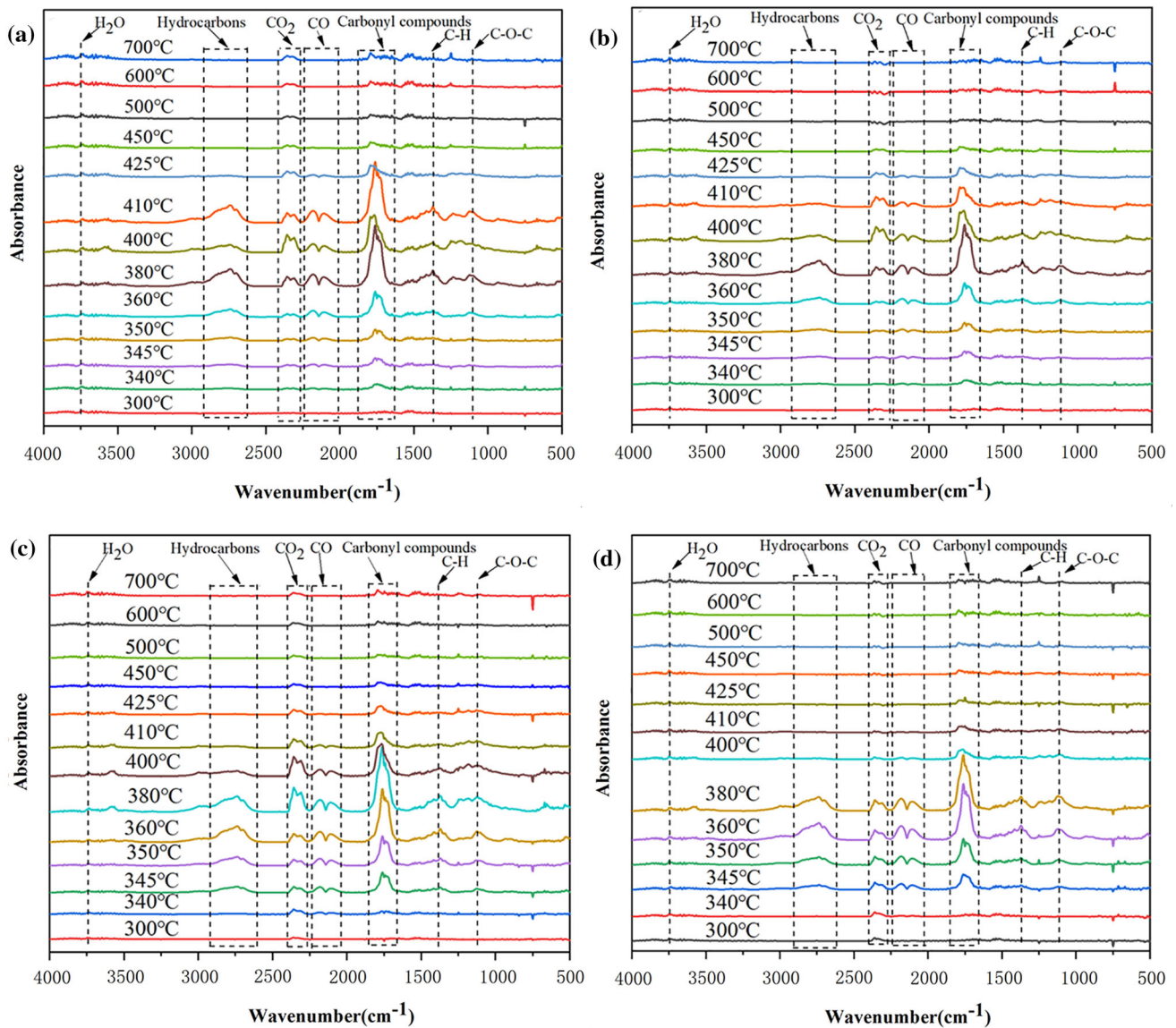


Figure 12 TG-IR spectra of **a** neat PLA, **b** PLA/10wt%APP, **c** PLA/5wt%PZM and **d** PLA/10wt%APP/5wt%PZM at different temperatures.

the PLA, which can effectively interrupt the pyrolysis process and inhibit the thermal degradation of the PLA [48–50].

Plausible flame-retardant mechanism

Figure 16 shows a schematic illustration of the flame-retardant mechanism of the PLA/10%APP/5%PZM. During the heating and combustion process, the APP dispersed in the PLA matrix is heated and decomposed to produce polyphosphoric acid and NH_3 . NH_3 can dilute the oxygen concentration around the

composite and bring away the heat flow, which is the so-called gas-phase flame retardancy.

In addition, the intermolecular dehydration occurs for the PLA caused by the catalysis of acidic substances to form a carbon layer covering the surface of the PLA matrix, which plays a crucial role in the insulation of the oxygen and heat, drip prevention and smoke suppression to achieve the effect of the condensed-phase flame retardance. With an increase in the temperature, the polyphosphoric acid will dehydrate and polymerize by itself, and the PLA will react with phosphoric acid and polyphosphoric acid to form the crosslinking structure [49–51]. The PZM

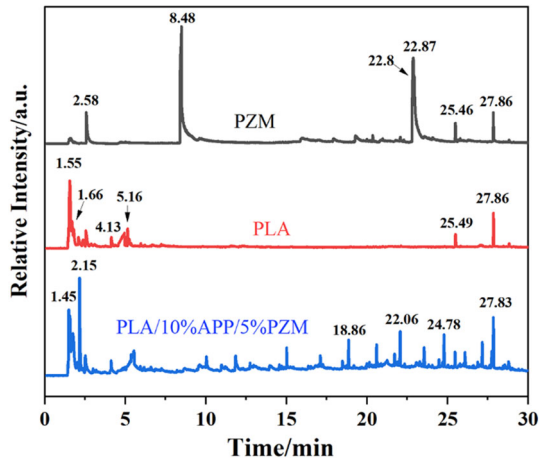


Figure 13 Total ion chromatograms of the PZM, neat PLA and PLA/10%APP/5%PZM in the PY-GC/MS test.

will be thermally degraded into two phosphazene units, producing some cross-linked carbon residues with the polyphosphoric acid. During the combustion process, a portion of the PLA molecular chains will be completely decomposed to generate CO, CO₂ and H₂O, which can also exert a gas-phase flame-retardant effect.

Crystallization behavior by DSC

PLA is a semicrystalline polyester with slow crystallization process and poor heat resistance. Figure 17 displays the non-isothermal/subsequent heating and isothermal crystallization curves of neat PLA and PLA/10%APP/5%PZM. No crystallization peak (P_c) could be found for neat PLA, and the P_c was discernible in the PLA/10%APP/5%PZM, PLA/10%APP and PLA/5%PZM (Fig. 17a). It suggests that the FRs enhanced the crystallizability of the PLA. In the subsequent heating curves (Fig. 17b), neat PLA presented a glass transition temperature (T_g), an extremely weak and wide cold crystallization peak (P_{cc}) and a melting peak (P_m) with a moderate intensity. With loading of the FRs, there were a T_g , obvious P_{cc} and high-intensity P_m , revealing the enhanced degree of the crystallinity or perfection of molecular chain alignment of the PLA. The relative degree of the crystallinity (X_c) of neat PLA and PLA with FRs is based on the following analytical procedure. $X_c = (\Delta H_m / \Delta H_m^0) \times 100\%$, in which $\Delta H_m = (\Delta H_m + \Delta H_{cc} + \Delta H_{rc})$ and ΔH_m^0 is ΔH_m (93.6 J/g [52]) of an infinitely large crystal of the PLA. ΔH_m , ΔH_{cc} and ΔH_{rc} are the enthalpy of melting, cold

crystallization and recrystallization in Fig. 17b, respectively. The X_c of neat PLA, PLA/10%APP, PLA/5%PZM and PLA/10%APP/5%PZM is 18.4%, 21.9%, 25.3% and 28.8%, respectively. In the isothermal crystallization process at $T_c = 110$ (Fig. 17c) and 130 °C (Fig. 17d), no P_c was seen in neat PLA. Upon incorporation of the FRs, the distinct P_c could be found, indicating that the crystallization of the PLA was significantly accelerated by FRs. It is noteworthy that the isothermal crystallization time of the PLA/10%APP/5%PZM is slightly lower than those of PLA/10%APP and PLA/5%PZM, indicating that the crystallization rate of the PLA/10%APP/5%PZM is the highest.

The enhanced X_c and crystallizability of the PLA are probably attributed to the nucleation effect of the APP/PZM. The APP/PZM synergistic FR also acts as the nucleating agent to provide large amount of nucleation sites to induce the nucleation of the PLA molecules and initiate the subsequent growth of the molecular chains.

Tensile measurement

The mechanical properties of neat PLA and three PLA-based composites are presented in Fig. S4. The elongation at break of PLA-based composite (PLA/10%APP, PLA/5%PZM and PLA/10%APP/5%PZM) decreased, compared to neat PLA, mainly ascribed to the non-uniform dispersion or agglomeration of the flame retardant. No obvious change could be found for the tensile strength. The detailed data on the mechanical property are listed in Table S3. It was reported that the mechanical properties of polymer-based composite with spherical filler strongly depend on the particle size and dispersion of dispersed phase, and interfacial interaction [53].

Conclusions

Synthesized PZM was a hyperbranched amorphous compound with the microsphere structure and showed a much higher thermal stability than the HCCP or ODA. Upon incorporation of the synergistic flame-retardant APP/PZM, the composites reached the V-0 rating in the UL-94 test and presented a substantially higher char residue amount than neat PLA. In the CONE measurement, the PLA/10%APP/5%PZM presented the most excellent flame-retardant

Figure 14 MS chromatograms of the PZM, neat PLA and PLA/10%APP/5%PZM at different retention times.

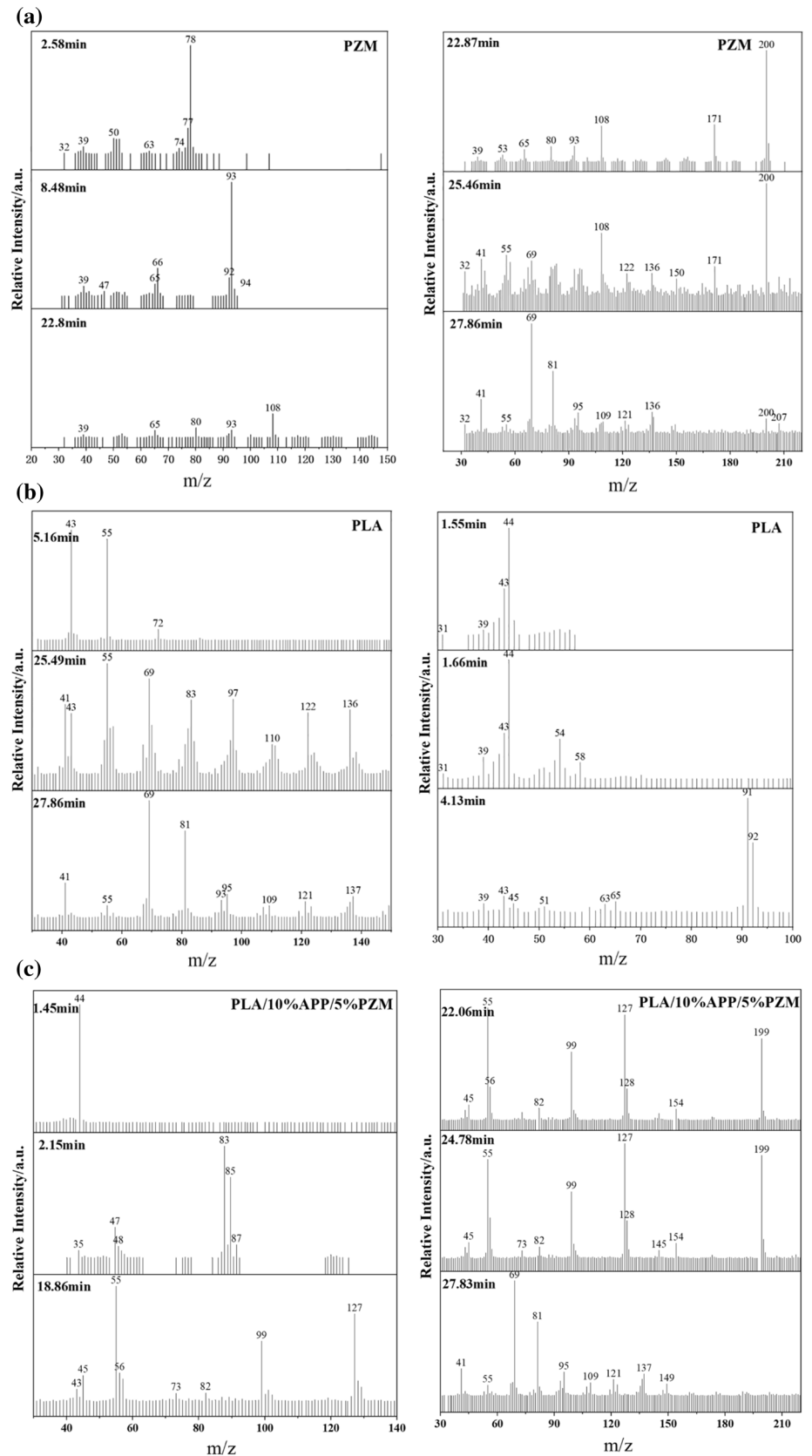
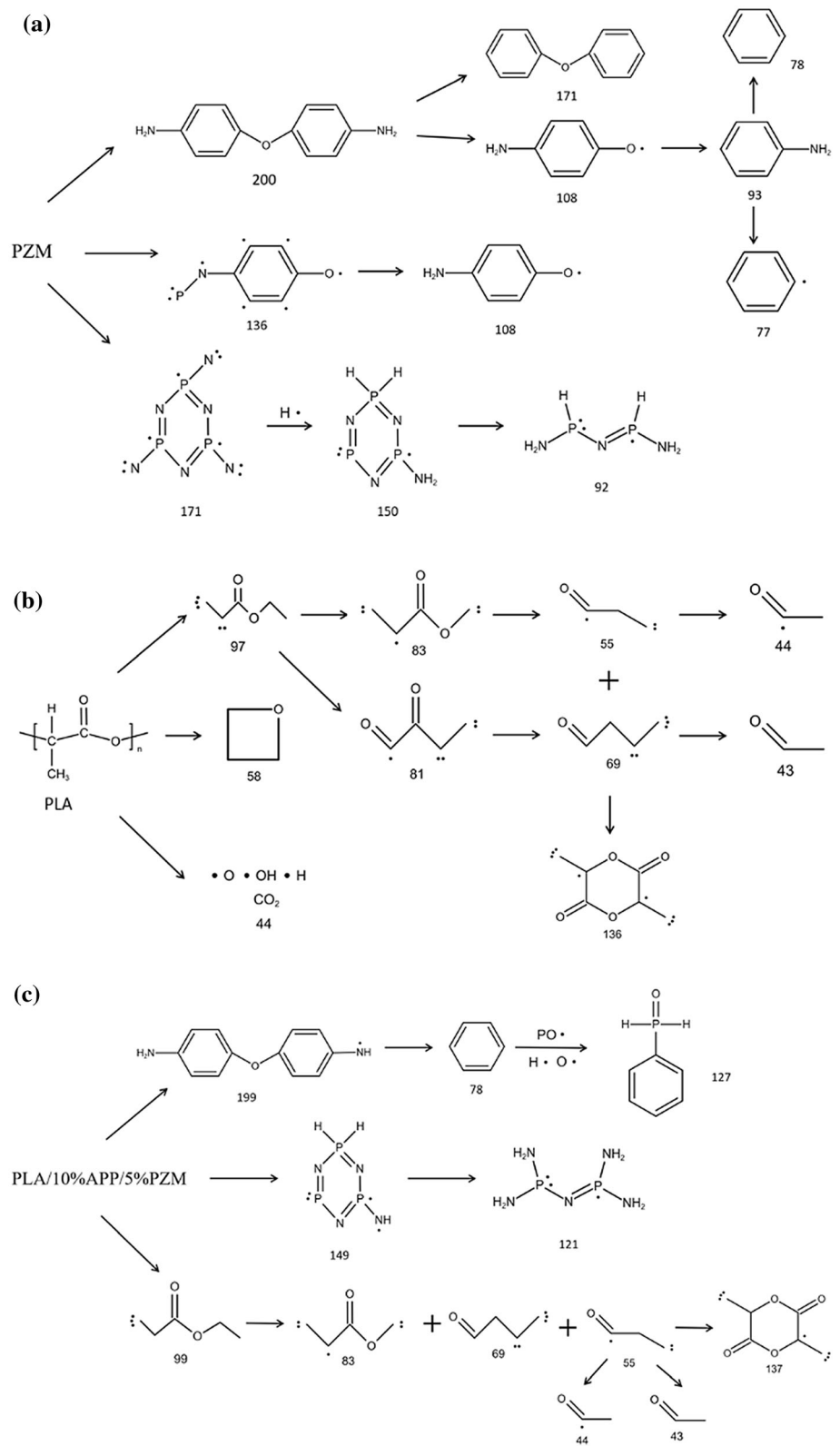


Figure 15 Possible pyrolysis processes of **a** the PZM, **b** neat PLA and **c** PLA/10%APP/5%PZM.



performance. The pHRR of the PLA/10%APP/5%PZM decreased by 27.2%, compared to neat PLA.

Also, the THR and TSR of the PLA/10%APP/5%PZM reduced significantly. The TTI and FRI value

Figure 16 Schematic illustration of the mechanism for the flame retardance.

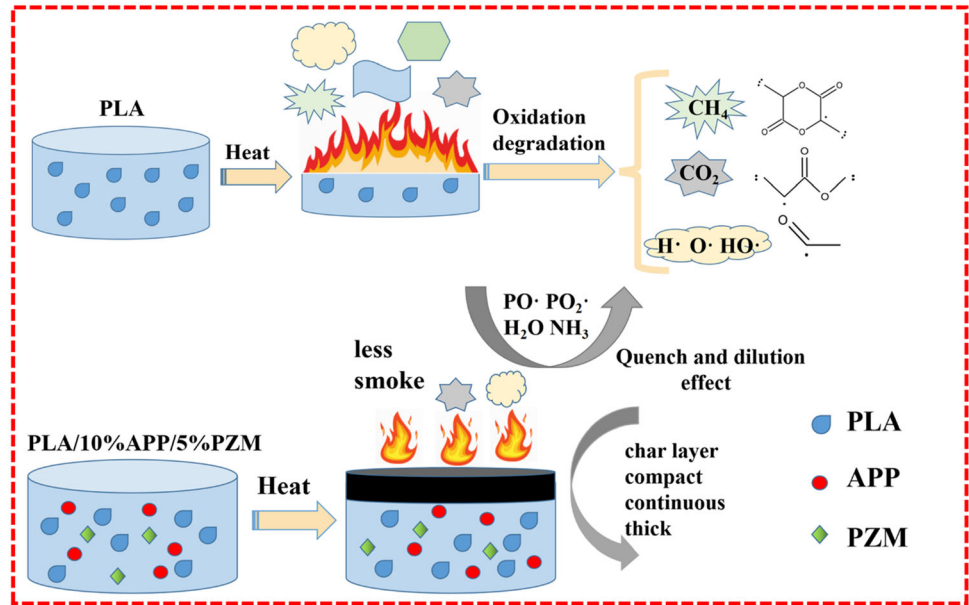
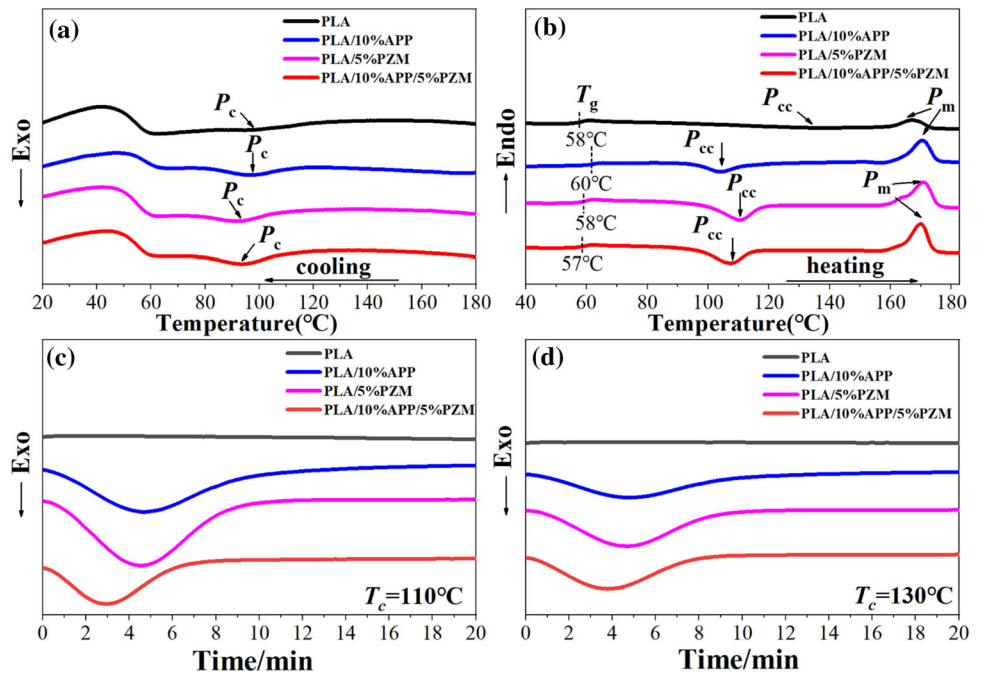


Figure 17 DSC curves of neat PLA and the PLA/FRs.



indicates that the PLA/10%APP/5%PZM had a high fire resistance and longer escaping time in the fire. TG-IR results suggest that the PLA/10%APP/5%PZM degraded earlier than neat PLA, resulting in the formation of the char layer. That is, the outstanding flame retardance of the PLA/10%APP/5%PZM was predominantly attributed to the formed continuous, dense and thicker char layer around the PLA/10%APP/5%PZM composite (condensed-phase flame retardance), which facilitates the insulation of

the oxygen and heat flow, suppression of the smoke and prevention of the dripping. In addition, the gas-phase flame retardance was minor factor to enhance the flame-retardant performance. The generated NH_3 , CO and CO_2 in the combustion process could dilute the oxygen concentration and bring away the heat. With loading of the 10%APP/5%PZM, the crystallizability of the PLA increased and the crystallization time shortened substantially, but the elongation at break decreased.

Acknowledgements

This work was financially supported by the “National Natural Science Foundation of China (41907329)” and “Natural Science Foundation of Tianjin City (20JCYBJC00580).”

Declarations

Conflict of interest The authors declare no any competing financial interest.

Supplementary Information: The online version contains supplementary material available at <http://doi.org/10.1007/s10853-021-06719-y>.

References

- He W, Song P, Yu B, Fang Z, Wang H (2020) Flame retardant polymeric nanocomposites through the combination of nanomaterials and conventional flame retardants. *Prog Mater Sci* 114:100687
- Liu H, Chen N, Shan P, Song P, Liu X, Chen J (2019) Toward fully bio-based and supertough PLA blends via in situ formation of cross-linked polyamide continuity network. *Macromolecules* 52:8415–8429
- Yang H, Yu B, Xu X, Bourbigot S, Wang H, Song P (2020) Lignin-derived bio-based flame retardants toward high-performance sustainable polymeric materials. *Green Chem* 22:2129–2161
- Kai D, Tan MJ, Chee PL, Chua YK, Yap YL, Loh XJ (2016) Towards lignin-based functional materials in a sustainable world. *Green Chem* 18:1175–1200
- Zhang Y, Jing J, Liu T, Xi L, Sai T, Ran S, Fang Z, Huo S, Song P (2021) A molecularly engineered bioderived polyphosphate for enhanced flame retardant, UV-blocking and mechanical properties of poly(lactic acid). *Chem Eng J* 411:128493
- Zhou Y, Tawiah B, Noor N, Zhang Z, Sun J, Yuen RKK, Fei B (2021) A facile and sustainable approach for simultaneously flame retarded, UV protective and reinforced poly(lactic acid) composites using fully bio-based complexing couples. *Compos Part B* 215:108833
- Laoutid F, Vahabi H, Shabani M, Aryanasab F, Zarrintaj P, Saeb MR (2018) A new direction in design of bio-based flame retardants for poly(lactic acid). *Fire Mater* 42:914–924
- Vahabi H, Shabani M, Aryanasab F, Mangin R, Laoutid F, Saeb MR (2018) Inclusion of modified lignocellulose and nano-hydroxyapatite in development of new bio-based adjuvant flame retardant for poly(lactic acid). *Thermochim Acta* 666:51–59
- Dorgan JR, Lehermeier HJ, Palade LI, Cicero J (2001) Polylactides: properties and prospects of an environmentally benign plastic from renewable resources. *Macromol Symp* 175:55–66
- Tsuji H (2016) Poly(lactic acid) stereocomplexes: a decade of progress. *Adv Drug Deliver Rev* 107:97–135
- Wen X, Liu Z, Li Z, Zhang J, Wang D, Szymanska K, Chen X, Mijowska E, Tang T (2020) Constructing multifunctional nanofiller with reactive interface in PLA/CBg-DOPO composites for simultaneously improving flame retardancy, electrical conductivity and mechanical properties. *Compos Sci Technol* 188:107988
- Jing J, Zhang Y, Fang Z, Wang D (2018) Core-shell flame retardant/graphene oxide hybrid: a self-assembly strategy towards reducing fire hazard and improving toughness of polylactic acid. *Compos Sci Technol* 165:161–167
- Zhang Y, Han P, Fang Z (2018) Synthesis of phospholipidated β -cyclodextrin and its application for flame-retardant poly(lactic acid) with ammonium polyphosphate. *J Appl Polym Sci* 135:46054
- Ran S, Fang F, Guo Z, Song P, Cai Y, Fang Z, Wang H (2019) Synthesis of decorated graphene with P, N-containing compounds and its flame retardancy and smoke suppression effects on polylactic acid. *Compos Part B* 170:41–50
- Chow WS, Teoh EL, Karger-Kocsis J (2018) Flame retarded poly(lactic acid): a review. *Express Polym Lett* 12:396–417
- Yuan X, Wang D, Chen L, Wang X, Wang Y (2011) Inherent flame retardation of bio-based poly(lactic acid) by incorporating phosphorus linked pendent group into the backbone. *Polym Degrad Stabil* 96:1669–1675
- Huo S, Yang S, Wang J, Cheng J, Zhang Q, Hu Y, Ding G, Zhang Q, Song P (2020) A liquid phosphorus-containing imidazole derivative as flameretardant curing agent for epoxy resin with enhanced thermal latency, mechanical, and flame-retardant performances. *J Hazard Mater* 386:121984
- Dasari A, Yu Z, Cai G, Mai Y (2013) Recent developments in the fire retardancy of polymeric materials. *Prog Polym Sci* 38:1357–1387
- Huang G, Huo S, Xu X, Chen W, Jin Y, Li R, Song P, Wang H (2019) Realizing simultaneous improvements in mechanical strength, flame retardancy and smoke suppression of ABS nanocomposites from multifunctional graphene. *Compos Part B* 177:107377
- Wang D, Song Y, Lin L, Wang L, Wang Y (2011) A novel phosphorus-containing poly(lactic acid) toward its flame retardation. *Polymer* 52:233–238
- Wei L, Wang D, Chen H, Chen L, Wang X, Wang Y (2011) Effect of a phosphorus-containing flame retardant on the

- thermal properties and ease of ignition of poly(lactic acid). *Polym Degrad Stabil* 96:1557–1561
- [22] Liu H, Wang X, Wu D (2014) Novel cyclotriphosphazene-based epoxy compound and its application in halogen-free epoxy thermosetting systems: Synthesis, curing behaviors, and flame retardancy. *Polym Degrad Stabil* 103:96–112
- [23] Jin W, Yuan L, Liang G, Gu A (2014) Multifunctional cyclotriphosphazene/hexagonal boron nitride hybrids and their flame retarding bismaleimide resins with high thermal conductivity and thermal stability. *ACS Appl Mater Inter* 6:14931–14944
- [24] Fu J, Xu Q, Chen J, Chen Z, Huang X, Tang X (2010) Controlled fabrication of uniform hollowcore porous shell carbon spheres by the pyrolysis of core/shell polystyrene/cross-linked polyphosphazene composites. *Chem Commun* 46:6563–6565
- [25] Zhu L, Xu Y, Yuan W, Xi J, Huang X, Tang X, Zheng S (2006) One-pot synthesis of poly(cyclotriphosphazene-co-4, 4'-sulfonyldiphenol) nanotubes via an in situ template approach. *Adv Mater* 18:2997–3000
- [26] Ke C, Li J, Feng K, Zhu Q, Zhu J, Yan Q, Wang Y (2010) Synergistic effect between a novel hyperbranched charring agent and ammonium polyphosphate on the flame retardant and anti-dripping properties of polylactide. *Polym Degrad Stabil* 95:763–770
- [27] Jin X, Cui S, Sun S, Gu X, Li H, Sun J, Zhang S, Bourbigot S (2019) The preparation of an intumescent flame retardant by ion exchange and its application in polylactic acid. *ACS Appl Polym Mater* 1:755–764
- [28] Chen Y, Wang W, Liu Z, Yao Y, Qian L (2019) Synthesis of a novel polyphosphazene/triazine bi-group flame retardant in situ doping nano zinc oxide and its application in poly (lactic acid) resin. *Polym Advan Technol* 30:1375–1385
- [29] Xu L, Wu X, Li L, Chen Y (2019) Synthesis of a novel polyphosphazene/triazine bi-group flame retardant in situ doping nano zinc oxide and its application in poly (lactic acid) resin. *Polym Adv Technol* 30:1375–1385
- [30] Chen Y, Xu L, Wu X, Xu B (2019) The influence of nano ZnO coated by phosphazene/triazine bi-group molecular on the flame retardant property and mechanical property of intumescent flame retardant poly (lactic acid) composites. *Thermochim Acta* 679:178336
- [31] Chen Y, He J, Xu L, Xu B, Qian L (2021) Mechanical properties and flame retardancy of PLA composites containing zinc oxide and chain extender. *J Appl Polym Sci* 138:50987
- [32] Wu N, Fu G, Yang Y, Xia M, Yun H, Wang Q (2019) Fire safety enhancement of a highly efficient flame retardant poly (phenylphosphoryl phenylenediamine) in biodegradable poly (lactic acid). *J Hazard Mater* 363:1–9
- [33] Yu T, Tuerhongjiang T, Sheng C, Li Y (2017) Phosphorus-containing diacid and its application in jute/poly (lactic acid) composites: mechanical, thermal and flammability properties. *Compos Part A-Appl S* 97:60–66
- [34] Jing J, Zhang Y, Tang X, Fang Z (2016) Synthesis of a highly efficient phosphorus-containing flame retardant utilizing plant-derived diphenolic acids and its application in poly lactic acid. *RSC Adv* 6:49019–49027
- [35] Costes L, Laoutid F, Dumazert L, Lopez-cuesta J, Brohez S, Delvosalle C, Dubois P (2015) Metallic phytates as efficient bio-based phosphorous flame retardant additives for poly (lactic acid). *Polym Degrad Stabil* 119:217–227
- [36] Liao F, Ju Y, Dai X, Cao Y, Li J, Wang X (2015) A novel efficient polymeric flame retardant for poly (lactic acid) (PLA): synthesis and its effects on flame retardancy and crystallization of PLA. *Polym Degrad Stabil* 120:251–261
- [37] Huang Y, Ma T, Wang Q, Guo C (2019) Synthesis of bio-based flame-retardant carboxylic acid curing agent and application in wood surface coating. *ACS Sustain Chem Eng* 7:14727–14738
- [38] Vahabi H, Shabaniyan M, Aryanasab F, Laoutid F, Benali S, Sabe MR, Seidi F, Kandola BK (2018) Three in one: β -cyclodextrin, nanohydroxyapatite, and a nitrogen-rich polymer integrated into a new flame retardant for poly(lactic acid). *Fire Mater* 42:593–602
- [39] Hu Y, Qiu S, Xing W, Feng X, Yu B, Mu X (2017) Self-standing cuprous oxide nanoparticles on silica@polyphosphazene nanospheres: 3D nanostructure for enhancing the flame retardancy and toxic effluents elimination of epoxy resins via synergistic catalytic effect. *J Hazard Mater* 309:802–814
- [40] Chen R, Luo Z, Yu X, Tang H, Zhou Y, Zhou H (2020) Synthesis of chitosan-based flame retardant and its fire resistance in epoxy resin. *Carbohydr Polym* 245:116530
- [41] Wu H, Zeng B, Chen J, Wu T, Li Y, Liu Y, Dai L (2019) An intramolecular hybrid of metal polyhedral oligomeric silsesquioxanes with special titanium-embedded cage structure and flame retardant functionality. *Chem Eng J* 374:1304–1316
- [42] Feng J, Xu X, Xu Z, Xie H, Song P, Li L, Huang G, Wang H (2020) One-Pot, solvent and catalyst-free synthesis of polyphosphoramidate as an eco-benign and effective flame retardant for poly (lactic acid). *ACS Sustain Chem Eng* 8:16612–16623
- [43] Ma Z, Liu X, Xu X, Liu L, Yu B, Maluk C, Huang G, Wang H, Song P (2021) Bioinspired, highly adhesive, nanostructured polymeric coatings for superhydrophobic fire-extinguishing thermal insulation foam. *ACS Nano*. <https://doi.org/10.1021/acsnano.1c02254>

- [44] Vahabi H, Kandola BK, Saeb MR (2019) Flame Retardancy Index for Thermoplastic Composites. *Polymers* 11:407
- [45] Zhang Y, Xiong Z, Ge H, Ni L, Zhang T, Huo S, Song P, Fang Z (2020) Core-shell bioderived flame retardants based on chitosan/alginate coated ammonia polyphosphate for enhancing flame retardancy of polylactic acid. *ACS Sustain Chem Eng* 8:6402–6412
- [46] Liu W, Chen D, Wang Y, Xing W, Bai Z, Lu H (2009) Flame retardancy and thermal degradation of intumescent flame retardant starch-based biodegradable composites. *Ind Eng Chem Res* 48:3150–3157
- [47] Song L, Xuan S, Wang X, Hu Y (2012) Flame retardancy and thermal degradation behaviors of phosphate in combination with POSS in polylactide composites. *Thermochim Acta* 529:1–7
- [48] Chen Y, Wang W, Qiu Y, Li L, Qian L, Xin F (2017) Terminal group effects of phosphazene-triazine bi-group flame retardant additives in flame retardant polylactic acid composites. *Polym Degrad Stabil* 140:166–175
- [49] Xue Y, Shen M, Zheng Y, Tao W, Han Y, Li W, Song P, Wang H (2020) One-pot scalable fabrication of an oligomeric phosphoramidate towards high-performance flame retardant polylactic acid with a submicron-grained structure. *Compos Part B* 183:107695
- [50] Zhang S, Yan Y, Wang W, Gu X, Li H, Li J, Sun J (2018) Intercalation of phosphotungstic acid into layered double hydroxides by reconstruction method and its application in intumescent flame retardant poly(lactic acid) composites. *Polym Degrad Stabil* 147:142–150
- [51] Yang W, Zhang H, Hu X, Liu Y, Zhang S, Xie C (2021) Self-assembled bio-derived microporous nanosheet from phytic acid as efficient intumescent flame retardant for polylactide. *Polym Degrad Stabil* 191:109664
- [52] Garlotta D (2001) A literature review of poly(lactic acid). *J Polym Environ* 9:63–84
- [53] Sun C, Mao H, Chen F, Fu Q (2018) Preparation of polylactide composite with excellent flame retardance and improved mechanical properties. *Chin J Polym Sci* 36:1385–1393

Publisher's Note Springer Nature remains neutral with regard to jurisdictional claims in published maps and institutional affiliations.